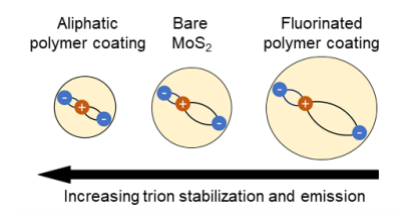
Stabilization of Three-Particle Excitations in Monolayer MoS₂ by Fluorinated Methacrylate Polymers

Nicholas Hight-Huf, $^{\dagger \S}$ James Nicolas Pagaduan, $^{\ddagger \S}$ Reika Katsumata, ‡ Todd Emrick, ‡ and Michael D. Barnes $^{\dagger = *}$

†Department of Chemistry, *Department of Physics, ‡Polymer Science and Engineering Department, University of Massachusetts, Amherst, MA 01003, USA *Corresponding Author, to whom all inquiries should be addressed §These authors contributed equally to this manuscript

Abstract

While extrinsic factors, such as substrates and chemical doping, are known to strongly influence visible photoemission from monolayer MoS₂, key fundamental knowledge for p-type polymeric dopants is lacking. We investigated perturbations to the electronic environment of 2D MoS₂ using fluorinated polymer coatings and specifically studied stabilization of three-particle states by monitoring changes in intensities and emission maxima of three-particle and two-particle emissions. We calculated changes in carrier density and trion binding energy, the latter having an additional contribution from MoS₂ polarization by the polymer. Polarization is further suggested by Kelvin probe force microscopy (KPFM) measurements of large Fermi level shifts. Changes similar in magnitude, but opposite in sign, were observed in 2D MoS₂ coated with an analogous non-fluorinated polymer. These findings highlight the important interplay between electron exchange and electrostatic interactions at the interface between polymers and transition metal dichalcogenides (TMDCs), which govern fundamental electronic properties relevant to next-generation devices.



Two-dimensional (2D) materials, such as monolayer MoS₂, possess outstanding electronic properties that are of interest for several next-generation devices, including ultrathin transistors, ^{1–} ³ photodetectors, ^{4–6} sensors, ^{7,8} and valleytronics. ^{9–11} Three-particle excitations are unique in 2D MoS₂ and structurally related TMDCs due to the significant association energy (on the order of 30 to 40 meV) between the exciton and the additional charge. 12 This binding energy reflects trion stabilization influenced by intrinsic and extrinsic factors that affect the Coulombic many-body interactions, which in turn dictate fundamental optoelectronic properties of the 2D material. Observations of trion behavior by photoluminescence (PL) spectroscopy lend quantitative insights into band structure, ^{12–15} in-plane and out-of-plane electronic screening, ¹⁶ vibrational excitations, ^{17–} ¹⁹ and transport properties. ^{20,21} A growing body of research describes the impact of fundamental materials properties (i.e., intrinsic factors), such as carrier density via electrical gating in a fieldeffect transistor arrangement, ^{12,15,22,23} and variations in crystal structure. ²⁴ Although the impacts of interactions with the surroundings (i.e., extrinsic factors) on trion behavior such as substrate, ^{17,25,26} defects, ^{27–29} strain, ^{19,30,31} gases, ³² and chemical (surface) doping ^{14,33,34} have been investigated extensively, the connection between p-type dopants³⁵ (particularly polymeric versions) and trion behavior is relatively unexplored.

Researchers have found trions in TMDCs to be useful for characterizing doping due to the inherent connection between carrier density and trion PL intensity. ^{12,13,15} In semiconductors, trion refers to the weakly bound three-body states resulting from the association of either an excess electron or an excess hole with a photogenerated electron-hole pair (*i.e.*, an exciton). In most materials, the binding energy of trions is so low that their existence is transient and becomes significant only at very low temperatures. However, MoS2 possesses a large trion binding energy, permitting characterization via room-temperature PL spectroscopy, which we employed here to assess doping by polymer coatings. Although at low temperatures distinct peaks corresponding to emission from excitons and trions are apparent, at room temperature a single emission envelope is observed due to homogeneous broadening of both peaks. Deconvolution of room-temperature PL into excitonic and trionic contributions is aided by the characteristic asymmetric shape of the trion peak. Particularly, the low-energy region of the trion peak exhibits a gradual exponential decrease in intensity as a result of the conservation of momentum between the emitted photon and the residual electron, termed electron recoil. ¹² A correlation between changes in trion behavior and changes in carrier density due to extrinsic factors such as adsorbed dopants has been established

using electrical gating experiments, demonstrating the utility of optical characterization for probing variation in carrier density.³⁶ Additionally, changes in trion binding energy have been used to probe carrier density,³⁷ dielectric screening from the surrounding environment,³⁸ and screening within the monolayer.^{39,40} Combined with the previous technique which relates the relative intensity of trion emission to carrier density, observations of the trion binding energy can be used to rationalize changes in effective screening in the material due to doping, a key consideration for sensors and for identifying charged impurities or inhomogeneities in the material which affect transport.

Herein, we investigated the stabilization of trions in 2D MoS₂ by its contact with fluorinated and non-fluorinated methacrylate-based polymer coatings, using PL spectroscopy to determine changes in trion population, carrier density, and trion binding energy, and correlating results with KPFM measurements of the Fermi level. We specifically probed whether polymers with strongly electronegative fluorinated pendent groups produce a significant increase in the excitonic emission of MoS₂ by inhibiting trion emission. To test this, reversible addition-fragmentation chain transfer (RAFT) polymerization was performed to prepare two polymers, namely poly(1H,1H,2H,2H-tridecafluoro-n-octyl methacrylate) (PTDFOMA) and poly(n-octyl methacrylate) (POMA), as shown in **Figure 1a**, which differ only by the presence of fluorine atoms in the sidechains of the former. Monolayer MoS₂ was grown by chemical vapor deposition and transferred to gold substrates (100 nm Au/10 nm Ti/300 nm SiO₂/Si), after which the polymers were applied by spin-coating (**Figure 1a**). Using PL and KPFM measurements, we observed that perfluorinated PTDFOMA films decreased the trion binding energy and increased the ratio of exciton-to-trion emission from monolayer MoS₂, while the non-fluorinated POMA led to an opposite n-doping effect.

PL measurements were performed on monolayer MoS₂, either bare or coated with one of the polymeric methacrylates (**Figure 1a**), where the polymer film thickness was estimated to be ~8 nm (see supporting information for details). The PL from 2D MoS₂ samples coated with PTDFOMA (normalized to unit area to aid comparisons) and excited with a 488-nm source increased markedly relative to those coated with POMA (**Figure 1b**). We also observed a slight decrease in intensity for the coated samples compared to bare MoS₂ (raw data are shown in **Figure S4**), attributed to scattering losses at the polymer-2D interface and, to a lesser extent, absorption

of light by the polymer. The PTDFOMA coating resulted in a blueshift and slight narrowing of the A exciton emission feature (*i.e.*, the transition between the conduction band and the higher energy valence band), whereas POMA resulted in a redshift and peak broadening.

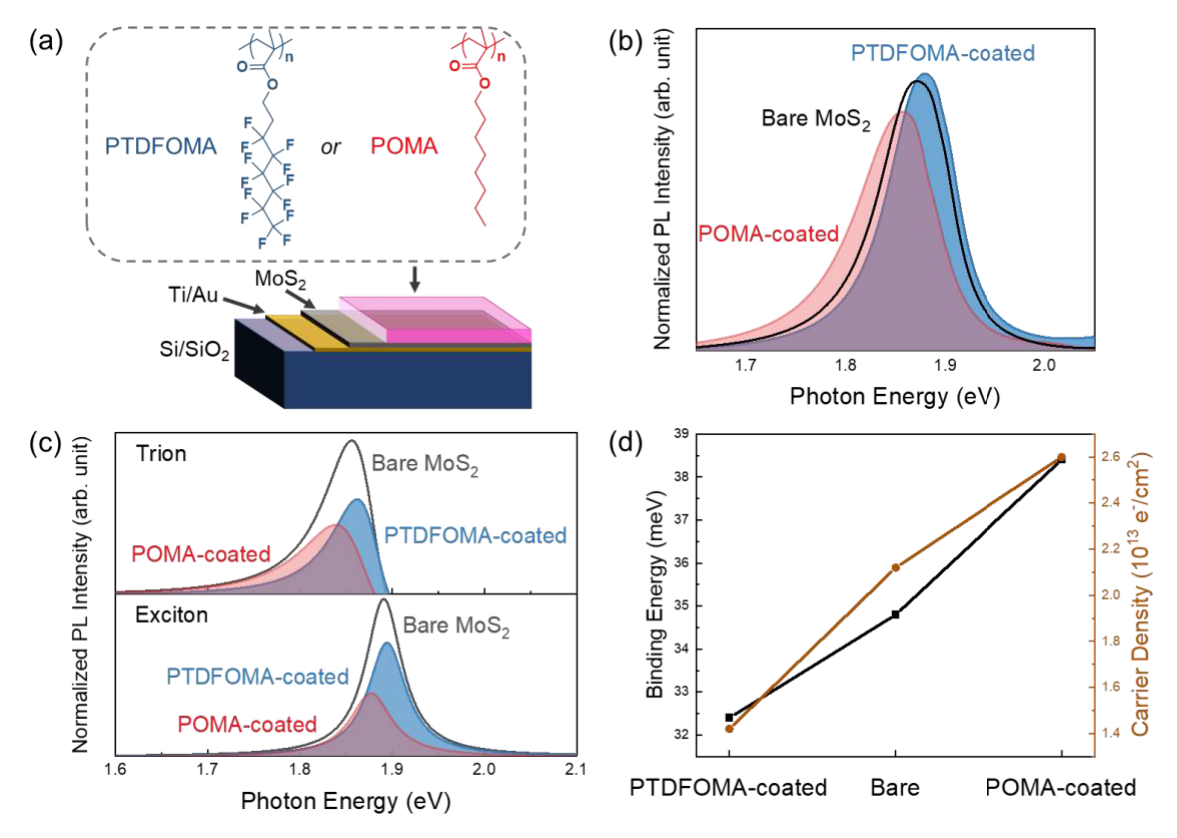


Figure 1. (a) Chemical structures of PTDFOMA and POMA, and the 2D MoS_2 sample configuration. (b) Changes in the photoluminescence of monolayer MoS_2 due to perfluorinated and non-fluorinated polymer treatment. (c) Fits to PL data, including contributions from exciton and trions. (d) Trends in binding energy and carrier density in bare and polymer-treated samples.

The factors affecting the PL shape and position become clear when the emission envelope is decomposed into contributions from exciton and trion emission (**Figure 1c**). While excitonic emission is expected to be fitted well solely by a Lorentzian lineshape function, trion emission must also account for the momentum of the remaining electron following radiative recombination, *i.e.*, electron recoil. The trion lineshape is approximated well by a decaying exponential as a consequence of a momentum-dependent decay rate and a thermal Boltzmann distribution of trion kinetic energy. When lifetime broadening (due to the uncertainty relation for energy which applies here to an excited state with a finite lifetime) is also accounted for, the result is the convolution of an exponential with a Lorentzian function. For fitting, we employed the following

analytical lineshape function discussed by Christopher *et al.*,¹² which is the result of a 1st order series approximation of the convolution integral, prior to integration:

$$I(E) = \frac{\Gamma}{\pi} \frac{1}{(E_{tr} - E)^2 + \Gamma^2} \left(1 + \frac{2\varepsilon (E_{tr} - E)}{(E_{tr} - E)^2 + \Gamma^2} \right)$$
(1)

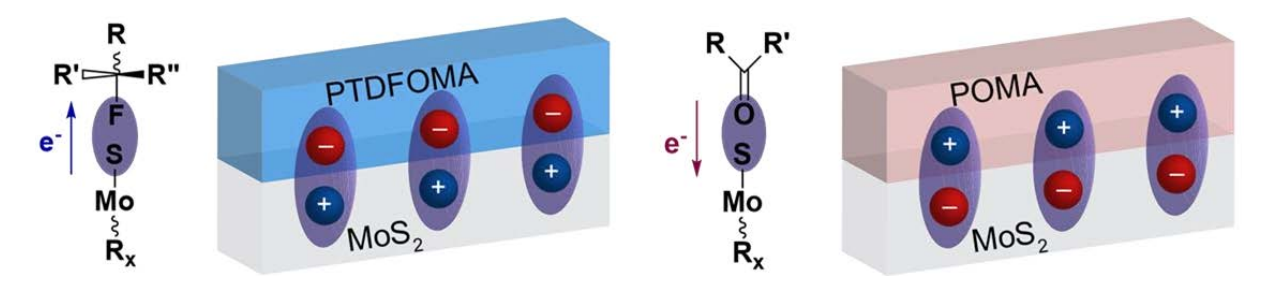
where Γ is the Lorentzian width parameter, E_{tr} is the zero-momentum transition energy, E is the emission energy, and ε is a parameter which controls the amount of exponential character (see supporting information for details of fitting).

Following decomposition into excitonic and trion contributions, the overall PL intensity profile can be understood not just in terms of differences between the relative weights of these two components, but also in terms of differences in their shape. Trion binding energy was evaluated by the difference in exciton and trion peak maxima. In bare MoS₂, excitonic emission is responsible for the majority of PL intensity. However, trion peak area is comparable to exciton peak area in POMA-coated MoS₂, which explains the redshift of the total PL. In the PTDFOMA-coated sample, the trion contribution to the total PL intensity was reduced compared to bare MoS₂, leading to a blueshift and a narrowing of the total emission envelope. Changes in the excitonic peak include a slight broadening in both polymer-treated samples (Figure 1c), associated with an increased lifetime and a large reduction in intensity in the POMA-coated sample, due to competition with trion emission. Under normal conditions, 2D MoS₂ has excess electrons which favor the formation of negative trions (*i.e.*, an exciton with an additional bound electron). Thus, as electron density increases, the probability of excitons forming trions prior to emission increases.

The ratios of trion peak area to total PL area can be related to the free carrier density in the 2D MoS₂ samples, examined here using the analysis of Mouri¹⁴ and Ross¹⁵ that employs the mass action law associated with trion formation and decay. We found that carrier density decreased from a nominal density of 2.12×10^{13} e⁻/cm² in bare MoS₂ to 1.42×10^{13} e⁻/cm² due to PTDFOMA coating (p-doping) and increased to 2.60×10^{13} e⁻/cm² due to POMA treatment (n-doping), as shown in **Figure 1d**. The observation of p-doping in PTDFOMA is attributed to the strong electronegativity of the perfluorinated moieties. With only limited experimental evidence available⁴¹ showing doping effects from polymers with weakly electron donating/withdrawing groups, we hypothesized that POMA would show no significant effects on electron density. Due

to the lack of electron-donating ability of linear alkanes, we reason that any donation is more likely to come from the carbonyl groups in the polymer backbone.⁴²

We observed significant changes in the trion binding energy (**Figure 1d**), corresponding to a difference in peak position between exciton and trion, with an increase for the POMA-coated samples (38.4 meV vs. 34.8 meV for bare MoS₂), and a decrease for the PTDFOMA-coated samples (32.4 meV). Although shifts in the binding energy were expected based on changes in carrier density,³⁷ additional effects were observed arising from changes in dielectric environment above MoS₂ from air to polymer,³⁸ and from polarization effects which alter in-plane screening.^{39,40} Both samples should experience a binding energy decrease from an increased environmental dielectric constant, as compared to air. However, we see additional positive deviations from the carrier density trend for both polymers, which we attribute to polarization effects which are larger in magnitude than changes to the dielectric environment above MoS₂ (**Scheme 1**).



Scheme 1. The strongly electronegative fluorinated groups in PTDFOMA form surface dipoles with MoS_2 by attracting electron density from the sulfur atoms. Surface dipoles between POMA and MoS_2 form, following electron donation from oxygen to the sulfur atoms.

Changes in the shape of the trion peak are pronounced (**Figure 1c**) with a significant increase in the parameter ε for POMA-coated samples (+74.8%) and a decrease for PTDFOMA (-11.0%) compared to bare MoS₂ (see table S1), where ε controls the contribution from the low-energy tail portion of the fit function. In POMA-coated samples, this increased tail character can be rationalized in terms of a decreased screening radius (*i.e.*, stronger screening within the plane of MoS₂), which implies a decreased trion size, and an increased screening radius and trion size due to PTDFOMA. ^{12,39,40} The trion emission maximum is redshifted by an increase in ε , but also from an increase in Γ (possibly due to increased lifetime broadening), both of which contributed to an increased trion binding energy in POMA and with the opposite behavior leading to a decreased trion binding energy in PTDFOMA. We note that there are other contributions to the

renormalization of the binding energy, such as the surrounding dielectric environment¹³ and interactions with defects, ^{15,27} which are not examined in detail here.

To characterize electronic changes in 2D MoS₂ as a function of polymer composition, we employed KPFM, an electric force scanning probe technique used to determine the Fermi level of samples through the measurement of surface potential contrast (SPC), ^{43–45} which is defined as:

$$SPC = \frac{\boldsymbol{\Phi}_{probe} - \boldsymbol{\Phi}_{sample}}{\rho} \tag{2}$$

SPC tracks changes in work function (Φ_{sample}) by calibrating the probe's work function (Φ_{probe}), where e is the charge of an electron. Here, we used highly oriented pyrolytic graphite for calibration (see supporting information). The work function is defined as $\Phi = E_{vac} - E_F$, so changes to the Fermi level track changes in the carrier density. That is, an increased Fermi level is associated with an increased electron density (decreased Φ , indicative of n-doping), and a decreased Fermi level is associated with decreased electron density (increased Φ , indicative of p-doping).

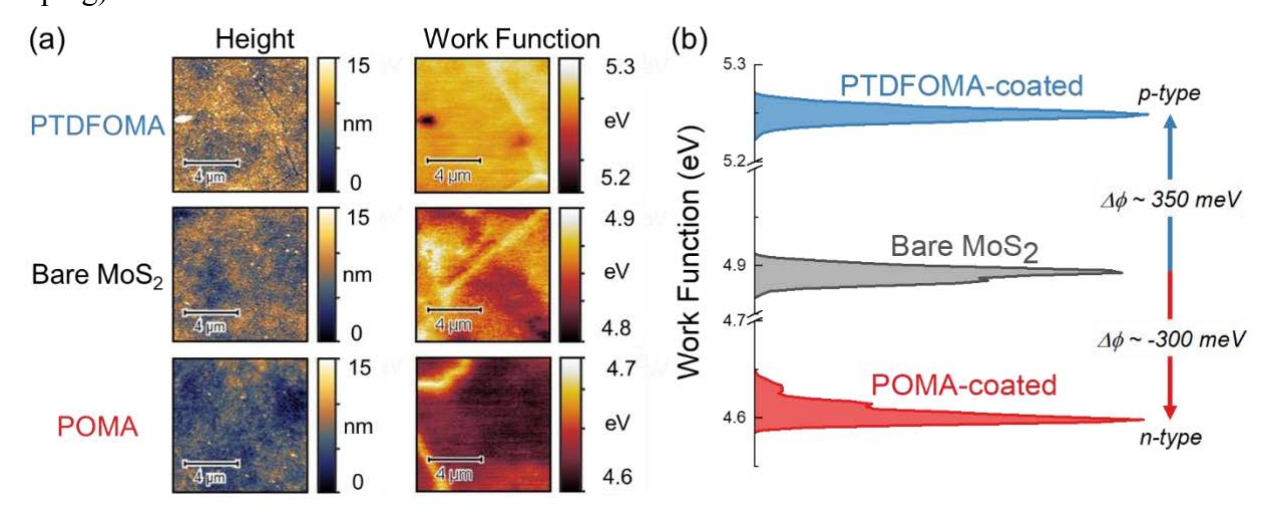


Figure 2. (a) KPFM height (left column) and surface potential (right column) images from PTDFOMA-coated, bare and POMA-coated MoS₂ samples. The height scale indicated by the color bar is 15 nm for all samples. (b) Work function distributions from KPFM measurements which show n-type doping by POMA and p-type doping by PTDFOMA. The lighter color (higher work function) lines in the KPFM images are breaks in the MoS₂ monolayer where the underlying gold substrate is exposed. Work function distributions in (b) do not include these exposed gold regions.

Performing KPFM under ambient conditions, we observed that the film quality of samples treated with both polymers is uniform in terms of surface coverage and roughness (**Figure 2a**). Work function maps (**Figure 2a**) of the same areas revealed bright colored (*i.e.*, higher Φ) lines,

which were interpreted as grain boundaries and removed from the analysis. The work function is shifted by the application of polymer films from a nominal value of 4.9 eV for bare MoS₂ (on Au/Ti/SiO₂/Si) to 5.3 eV by PTDFOMA treatment (p-doping), and 4.6 eV by POMA treatment (n-doping), as illustrated in **Figure 2b**. We note that the magnitude of these shifts is substantial and in qualitative agreement with PL analysis, which estimated significant p- and n-doping effects from PTDFOMA and POMA, respectively.

To gain more perspective on the significance of these findings, we predicted the shift in the Fermi level by employing the parabolic band approximation to express the difference between the Fermi level and the conduction band edge:⁴⁶

$$E_F - E_c = k_b T \ln \left[Exp \left(\frac{n}{g_{2D} k_b T} \right) - 1 \right]$$
 (3)

where E_c is the conduction band energy, k_b is Boltzmann's constant, n is the sheet carrier density, and g_{2D} is the 2D density of states at the band edge. Using the carrier densities determined by the PL measurements, we predicted shifts in the Fermi level of ~ -10 meV for PTDFOMA (towards the valence band), and ~ 5 meV for POMA (towards the conduction band). The differences between the shifts measured by KPFM and those predicted from changes in carrier density as determined by PL were $\sim 40 \times$ and $60 \times$ for PTDFOMA and POMA, respectively. We attributed these discrepancies to significant dipole interactions which formed at the 2D-polymer interface and produced an additional, substantial shift in the Fermi energy, independent of any charge exchange between MoS₂ and the polymers. 42,47–49 This substantial shift in the Fermi energy, despite a modest shift in carrier density, reflects the powerful role that differences in electronegativity play in dipole formation that modifies the electronic environment of the 2Dpolymer interface. These dipole effects further modify trion behavior (binding energy), independent of carrier density changes. Overall, our findings reinforce the importance of polarization effects on the Coulombic many-body interactions that govern the optoelectronic properties of 2D MoS₂ and demonstrate an approach to quantitatively disentangle contributions from carrier density changes by using a combination of PL and KPFM. A similar approach would be useful to investigate quantitative aspects and mechanistic details pertaining to the surface modification of TMDCs in general by a variety of polymeric and non-polymeric coatings, the results of which will be pertinent to 2D materials device applications.

We found that methacrylate polymers with linear perfluorinated side chains as thin film coatings resulted in significant changes to the trion signatures in the PL spectra of monolayer MoS₂. Changes in electron density were significant, -0.70×10^{13} e⁻/cm² due to PTDFOMA and 0.48×10^{13} e⁻/cm² due to POMA, with changes in binding energy of \sim -2 and 4 meV, respectively. Significant shifts in the Fermi level of monolayer MoS₂ were measured by KPFM, which is interpreted as strongly dipole-driven based on the insufficient changes in carrier density needed to achieve such shifts. From this, we conclude that contact of the perfluorinated sidechains with MoS₂ results in the observed changes in electron density and Fermi level. Thus, the strong effects on trion stabilization by perfluorinated and non-fluorinated methacrylate polymers arise from both charge exchange and dipole effects, as deduced by KPFM measurements. This demonstrates the sensitivity of trion stabilization to factors that influence the electronic properties of devices based on TMDCs, such as carrier density and polarization. We have additionally shown the utility of perfluorinated polymer coatings as p-type dopants of MoS₂, and their contrasting electronic impact to that of a non-fluorinated analogue. Future work will broaden the scope of polymer and TMDC compositions studied in this manner.

Associated Content

Supporting Information

Synthetic methods and characterization of the monomers and polymers, details of PL measurements and calculations, and details of KPFM, are available free of charge at http://pubs.acs.org.

Author Information

Corresponding Author

Michael D. Barnes - Department of Chemistry, Department of Physics, University of Massachusetts Amherst, Amherst, Massachusetts, 01003, United States. Email: mdbarnes@chem.umass.edu

Authors

Nicholas Hight-Huf – Department of Chemistry, University of Massachusetts Amherst, Amherst, Massachusetts, 01003, United States.

James Nicolas Pagaduan – Polymer Science and Engineering Department, University of Massachusetts Amherst, Massachusetts, 01003, United States.

Reika Katsumata - Polymer Science and Engineering Department, University of Massachusetts Amherst, Massachusetts, 01003, United States.

Todd Emrick - Polymer Science and Engineering Department, University of Massachusetts Amherst, Massachusetts, 01003, United States.

Author Contributions

§N.H.H. and J.N.P contributed equally to this manuscript.

Notes

The authors declare no competing financial interest.

Acknowledgements

We gratefully acknowledge the National Science Foundation (NSF-BSF 1808011) and the US-Israel Binational Science Foundation (2017655) for support. R.K. expresses gratitude for startup funding from UMass Amherst.

References

- (1) Wang, H.; Yu, L.; Lee, Y.-H.; Shi, Y.; Hsu, A.; Chin, M. L.; Li, L.-J.; Dubey, M.; Kong, J.; Palacios, T. Integrated Circuits Based on Bilayer MoS₂ Transistors. *Nano Lett.* **2012**, *12* (9), 4674–4680.
- (2) Late, D. J.; Liu, B.; Matte, H. S. S. R.; Dravid, V. P.; Rao, C. N. R. Hysteresis in Single-Layer MoS₂ Field Effect Transistors. *ACS Nano* **2012**, *6* (6), 5635–5641.

- (3) Liu, X.; Qu, D.; Ryu, J.; Ahmed, F.; Yang, Z.; Lee, D.; Yoo, W. J. P-Type Polar Transition of Chemically Doped Multilayer MoS₂ Transistor. *Adv. Mater.* **2016**, *28* (12), 2345–2351.
- (4) Lopez-Sanchez, O.; Lembke, D.; Kayci, M.; Radenovic, A.; Kis, A. Ultrasensitive Photodetectors Based on Monolayer MoS₂. *Nat. Nanotechnol.* **2013**, *8* (7), 497–501.
- (5) Wang, X.; Wang, P.; Wang, J.; Hu, W.; Zhou, X.; Guo, N.; Huang, H.; Sun, S.; Shen, H.; Lin, T.; et al. Ultrasensitive and Broadband MoS₂ Photodetector Driven by Ferroelectrics. *Adv. Mater.* **2015**, *27* (42), 6575–6581.
- (6) Li, S.; Chen, X.; Liu, F.; Chen, Y.; Liu, B.; Deng, W.; An, B.; Chu, F.; Zhang, G.; Li, S.; et al. Enhanced Performance of a CVD MoS₂ Photodetector by Chemical in Situ N-Type Doping. *ACS Appl. Mater. Interfaces* **2019**, *11* (12), 11636–11644.
- (7) Hang, Y.; Li, Q.; Luo, W.; He, Y.; Zhang, X.; Peng, G. Photo-Electrical Properties of Trilayer MoSe₂ Nanoflakes. *Nano* **2016**, *11* (07), 1650082.
- (8) Cheng, R.; Jiang, S.; Chen, Y.; Liu, Y.; Weiss, N.; Cheng, H.-C.; Wu, H.; Huang, Y.; Duan, X. Few-Layer Molybdenum Disulfide Transistors and Circuits for High-Speed Flexible Electronics. *Nat. Commun.* **2014**, *5* (1), 5143.
- (9) Cao, T.; Wang, G.; Han, W.; Ye, H.; Zhu, C.; Shi, J.; Niu, Q.; Tan, P.; Wang, E.; Liu, B.; et al. Valley-Selective Circular Dichroism of Monolayer Molybdenum Disulphide. *Nat. Commun.* **2012**, *3* (1), 887.
- (10) Mak, K. F.; He, K.; Shan, J.; Heinz, T. F. Control of Valley Polarization in Monolayer MoS₂ by Optical Helicity. *Nat. Nanotechnol.* **2012**, *7*, 494.
- (11) Zeng, H.; Dai, J.; Yao, W.; Xiao, D.; Cui, X. Valley Polarization in MoS₂ Monolayers by Optical Pumping. *Nat. Nanotechnol.* **2012**, *7* (8), 490–493.
- (12) Christopher, J. W.; Goldberg, B. B.; Swan, A. K. Long Tailed Trions in Monolayer MoS₂: Temperature Dependent Asymmetry and Resulting Red-Shift of Trion Photoluminescence Spectra. *Sci. Rep.* **2017**, *7* (1), 14062.
- (13) Mak, K. F.; He, K.; Lee, C.; Lee, G. H.; Hone, J.; Heinz, T. F.; Shan, J. Tightly Bound Trions in Monolayer MoS₂. *Nat. Mater.* **2013**, *12* (3), 207–211.

- (14) Mouri, S.; Miyauchi, Y.; Matsuda, K. Tunable Photoluminescence of Monolayer MoS₂ via Chemical Doping. *Nano Lett.* **2013**, *13* (12), 5944–5948.
- (15) Ross, J. S.; Wu, S.; Yu, H.; Ghimire, N. J.; Jones, A. M.; Aivazian, G.; Yan, J.; Mandrus, D. G.; Xiao, D.; Yao, W.; et al. Electrical Control of Neutral and Charged Excitons in a Monolayer Semiconductor. *Nat. Commun.* 2013, 4, 1–6.
- (16) Lin, Y.; Ling, X.; Yu, L.; Huang, S.; Hsu, A. L.; Lee, Y.-H.; Kong, J.; Dresselhaus, M. S.; Palacios, T. Dielectric Screening of Excitons and Trions in Single-Layer MoS₂. *Nano Lett.* 2014, *14* (10), 5569–5576.
- (17) Sarkar, S.; Goswami, S.; Trushin, M.; Saha, S.; Panahandeh-Fard, M.; Prakash, S.; Tan, S. J. R.; Scott, M.; Loh, K. P.; Adam, S.; et al. Polaronic Trions at the MoS₂/SrTiO₃ Interface. *Adv. Mater.* **2019**, *31* (41), 1903569.
- (18) Nguyen, P. X.; Garg, S.; Tse, W.-K.; Pan, S.; Kung, P.; Kim, S. M. Polarization Dependent Trion Dynamics in Large Area CVD Grown 2D Monolayer MoS₂ by Terahertz Time-Domain Spectroscopy. *J. Phys. D. Appl. Phys.* **2019**, *52* (15), 155104.
- (19) Michail, A.; Anestopoulos, D.; Delikoukos, N.; Parthenios, J.; Grammatikopoulos, S.; Tsirkas, S. A.; Lathiotakis, N. N.; Frank, O.; Filintoglou, K.; Papagelis, K. Biaxial Strain Engineering of CVD and Exfoliated Single- and Bi-Layer MoS₂ Crystals. 2D Mater. 2020, 8 (1), 15023.
- (20) Lui, C. H.; Frenzel, A. J.; Pilon, D. V.; Lee, Y.-H.; Ling, X.; Akselrod, G. M.; Kong, J.; Gedik, N. Trion-Induced Negative Photoconductivity in Monolayer MoS₂. *Phys. Rev. Lett.* **2014**, *113* (16), 166801.
- (21) Uddin, S. Z.; Kim, H.; Lorenzon, M.; Yeh, M.; Lien, D.-H.; Barnard, E. S.; Htoon, H.; Weber-Bargioni, A.; Javey, A. Neutral Exciton Diffusion in Monolayer MoS₂. *ACS Nano* **2020**, *14* (10), 13433–13440.
- (22) Lee, B.; Liu, W.; Naylor, C. H.; Park, J.; Malek, S. C.; Berger, J. S.; Johnson, A. T. C.; Agarwal, R. Electrical Tuning of Exciton–Plasmon Polariton Coupling in Monolayer MoS₂ Integrated with Plasmonic Nanoantenna Lattice. *Nano Lett.* **2017**, *17* (7), 4541–4547.
- (23) Luo, Z.; Jia, H.; Lv, L.; Wang, Q.; Yan, X. Gate-Tunable Trion Binding Energy in

- Monolayer MoS₂ with Plasmonic Superlattice. *Nanoscale* **2020**, *12* (34), 17754–17761.
- (24) Friedman, A. L.; Hanbicki, A. T.; Perkins, F. K.; Jernigan, G. G.; Culbertson, J. C.; Campbell, P. M. Evidence for Chemical Vapor Induced 2H to 1T Phase Transition in MoX2 (X = Se, S) Transition Metal Dichalcogenide Films. *Sci. Rep.* **2017**, *7* (1), 3836.
- (25) Drüppel, M.; Deilmann, T.; Krüger, P.; Rohlfing, M. Diversity of Trion States and Substrate Effects in the Optical Properties of an MoS₂ Monolayer. *Nat. Commun.* **2017**, *8* (1), 2117.
- (26) Paul, K. K.; Mawlong, L. P. L.; Giri, P. K. Trion-Inhibited Strong Excitonic Emission and Broadband Giant Photoresponsivity from Chemical Vapor-Deposited Monolayer MoS₂ Grown in Situ on TiO₂ Nanostructure. *ACS Appl. Mater. Interfaces* **2018**, *10* (49), 42812–42825.
- (27) Nan, H.; Wang, Z.; Wang, W.; Liang, Z.; Lu, Y.; Chen, Q.; He, D.; Tan, P.; Miao, F.; Wang, X.; et al. Strong Photoluminescence Enhancement of MoS₂ through Defect Engineering and Oxygen Bonding. *ACS Nano* **2014**, *8* (6), 5738–5745.
- (28) Zhao, W.; Ma, J.; Sun, P.; Zhang, K.; Yuan, Y. Strong Photoluminescence Enhancement of MoS₂ Monolayer via Low-Power Ar/O₂ Plasma Treatment. *Mater. Lett.* **2019**, *235*, 129–132.
- (29) Burns, K.; Tan, A. M. Z.; Gabriel, A.; Shao, L.; Hennig, R. G.; Aitkaliyeva, A. Controlling Neutral and Charged Excitons in MoS₂ with Defects. *J. Mater. Res.* **2020**, *35* (8), 949–957.
- (30) He, X.; Li, H.; Zhu, Z.; Dai, Z.; Yang, Y.; Yang, P.; Zhang, Q.; Li, P.; Schwingenschlogl, U.; Zhang, X. Strain Engineering in Monolayer WS₂, MoS₂, and the WS₂/MoS₂ Heterostructure. *Appl. Phys. Lett.* **2016**, *109* (17), 173105.
- (31) Michail, A.; Parthenios, J.; Anestopoulos, D.; Galiotis, C.; Christian, M.; Ortolani, L.; Morandi, V.; Papagelis, K. Controllable, Eco-Friendly, Synthesis of Highly Crystalline 2D-MoS₂ and Clarification of the Role of Growth-Induced Strain. 2D Mater. 2018, 5 (3), 35035.
- (32) Tongay, S.; Zhou, J.; Ataca, C.; Liu, J.; Kang, J. S.; Matthews, T. S.; You, L.; Li, J.; Grossman, J. C.; Wu, J. Broad-Range Modulation of Light Emission in Two-Dimensional Semiconductors by Molecular Physisorption Gating. *Nano Lett.* **2013**, *13* (6), 2831–2836.

- (33) Cadiz, F.; Tricard, S.; Gay, M.; Lagarde, D.; Wang, G.; Robert, C.; Renucci, P.; Urbaszek, B.; Marie, X. Well Separated Trion and Neutral Excitons on Superacid Treated MoS₂ Monolayers. *Appl. Phys. Lett.* **2016**, *108* (25), 251106.
- Obaidulla, S. M.; Habib, M. R.; Khan, Y.; Kong, Y.; Liang, T.; Xu, M. MoS₂ and Perylene Derivative Based Type-II Heterostructure: Bandgap Engineering and Giant Photoluminescence Enhancement. *Adv. Mater. Interfaces* **2020**, *7* (3), 1901197.
- (35) Su, W.; Dou, H.; Huo, D.; Dai, N.; Yang, L. Enhancing Photoluminescence of Trion in Single-Layer MoS₂ Using p-Type Aromatic Molecules. *Chem. Phys. Lett.* **2015**, *635*, 40–44.
- (36) Liu, B.; Zhao, W.; Ding, Z.; Verzhbitskiy, I.; Li, L.; Lu, J.; Chen, J.; Eda, G.; Loh, K. P. Engineering Bandgaps of Monolayer MoS₂ and WS₂ on Fluoropolymer Substrates by Electrostatically Tuned Many-Body Effects. *Adv. Mater.* **2016**, *28* (30), 6457–6464.
- (37) Lundt, N.; Cherotchenko, E.; Iff, O.; Fan, X.; Shen, Y.; Bigenwald, P.; Kavokin, A. V; Höfling, S.; Schneider, C. The Interplay between Excitons and Trions in a Monolayer of MoSe₂. *Appl. Phys. Lett.* **2018**, *112* (3), 31107.
- (38) Kylänpää, I.; Komsa, H.-P. Binding Energies of Exciton Complexes in Transition Metal Dichalcogenide Monolayers and Effect of Dielectric Environment. *Phys. Rev. B* **2015**, *92* (20), 205418.
- (39) Courtade, E.; Semina, M.; Manca, M.; Glazov, M. M.; Robert, C.; Cadiz, F.; Wang, G.; Taniguchi, T.; Watanabe, K.; Pierre, M.; et al. Charged Excitons in Monolayer WSe₂: Experiment and Theory. *Phys. Rev. B* **2017**, *96* (8), 85302.
- (40) Berkelbach, T. C.; Hybertsen, M. S.; Reichman, D. R. Theory of Neutral and Charged Excitons in Monolayer Transition Metal Dichalcogenides. *Phys. Rev. B* **2013**, *88* (4), 45318.
- (41) Liang, J.; Xu, K.; Toncini, B.; Bersch, B.; Jariwala, B.; Lin, Y.-C.; Robinson, J.; Fullerton-Shirey, S. K. Impact of Post-Lithography Polymer Residue on the Electrical Characteristics of MoS₂ and WSe₂ Field Effect Transistors. *Adv. Mater. Interfaces* **2019**, *6* (3), 1801321.
- (42) Pagaduan, J. N.; Hight-Huf, N.; Datar, A.; Nagar, Y.; Barnes, M.; Naveh, D.; Ramasubramaniam, A.; Katsumata, R.; Emrick, T. Electronic Tuning of Monolayer

- Graphene with Polymeric "Zwitterists." ACS Nano 2021, 15 (2), 2762–2770.
- (43) Selhorst, R. C.; Puodziukynaite, E.; Dewey, J. A.; Wang, P.; Barnes, M. D.; Ramasubramaniam, A.; Emrick, T. Tetrathiafulvalene-Containing Polymers for Simultaneous Non-Covalent Modification and Electronic Modulation of MoS(2) Nanomaterials. *Chem. Sci.* **2016**, *7* (7), 4698–4705.
- (44) Selhorst, R.; Wang, P.; Barnes, M.; Emrick, T. Bithiazolidinylidene Polymers: Synthesis and Electronic Interactions with Transition Metal Dichalcogenides. *Chem. Sci.* **2018**, *9* (22), 5047–5051.
- (45) Wang, P.; Selhorst, R.; Emrick, T.; Ramasubramaniam, A.; Barnes, M. D. Bidirectional Electronic Tuning of Single-Layer MoS₂ with Conjugated Organochalcogens. *J. Phys. Chem. C* **2019**, *123* (2), 1506–1511.
- (46) Ma, N.; Jena, D. Carrier Statistics and Quantum Capacitance Effects on Mobility Extraction in Two-Dimensional Crystal Semiconductor Field-Effect Transistors. *2D Mater.* **2015**, *2*.
- (47) Hight-Huf, N.; Nagar, Y.; Levi, A.; Pagaduan, J. N.; Datar, A.; Katsumata, R.; Emrick, T.; Ramasubramaniam, A.; Naveh, D.; Barnes, M. D. Polarization-Driven Asymmetric Electronic Response of Monolayer Graphene to Polymer Zwitterions Probed from Both Sides. *ACS Appl. Mater. Interfaces* **2021**.
- (48) Gobbi, M.; Bonacchi, S.; Lian, J. X.; Vercouter, A.; Bertolazzi, S.; Zyska, B.; Timpel, M.; Tatti, R.; Olivier, Y.; Hecht, S.; et al. Collective Molecular Switching in Hybrid Superlattices for Light-Modulated Two-Dimensional Electronics. *Nat. Commun.* **2018**, *9* (1), 2661.
- (49) Christodoulou, C.; Giannakopoulos, A.; Nardi, M. V; Ligorio, G.; Oehzelt, M.; Chen, L.; Pasquali, L.; Timpel, M.; Giglia, A.; Nannarone, S.; et al. Tuning the Work Function of Graphene-on-Quartz with a High Weight Molecular Acceptor. *J. Phys. Chem. C* 2014, 118 (9), 4784–4790.

SUPPORTING INFORMATION

Stabilization of Three-Particle Excitations in Monolayer MoS₂ by Fluorinated Methacrylate Polymers

Nicholas Hight-Huf,†§ James Nicolas Pagaduan,‡§ Reika Katsumata,‡ Todd Emrick,‡ and Michael D. Barnes†=*

†Department of Chemistry, Department of Physics, ‡Polymer Science and Engineering Department,
University of Massachusetts, Amherst, MA 01003, USA
*Corresponding author, to whom all inquiries should be addressed
§These authors contributed equally to this manuscript

Methods

Materials. CVD-grown MoS₂ monolayer continuous films (10 mm × 10 mm) on Au/Ti/SiO₂/Si and SiO₂/Si (300 nm oxide layer) were procured from 6Carbon Technology (Shenzhen, China). 1-Octanol (99%), methacryloyl chloride (97%), 2.2'-azobisisobutyronitrile 98%). 4-cvano-4-(AIBN, (phenylcarbonothioylthio)pentanoic acid, triethylamine (TEA, 99.0+%), dichloromethane (DCM, 99.8+%), and toluene (99.8+%) were purchased from Sigma-Aldrich (St. Louis, MO, USA). 2,2,2-trifluoroethanol (TFE, 99.9%) was obtained from Oakwood Products, Inc (West Columbia, SC, USA). Chloroform-d (99.8%) and 2,2,2-trifluoroethanol-d₃ (99%) were purchased from Cambridge Isotope Laboratories (Tewksbury, MA, USA). 1H,1H,2H,2H-Tridecafluoro-n-octyl methacrylate (TDFOMA, stabilized with MEHQ, 98.0+%) was obtained from Fisher Scientific (Waltham, MA, USA), and run through a plug of basic alumina to remove the inhibitor. Before use, AIBN was recrystallized from methanol. TEA and DCM were separately dried and distilled over calcium hydride. Toluene was dried and distilled over sodium/benzophenone. All other materials were used as received without additional purification.

Synthesis of n-Octyl Methacrylate Monomer. 1-Octanol (1.20 mL, 7.57 mmol) and triethylamine (1.28 mL, 9.18 mmol) were dissolved in anhydrous dichloromethane (15 mL) in a flame-dried 100-mL three-necked flask charged with a stir bar. The mixture was cooled in an ice/water bath for 10 min, and methacryloyl chloride (0.842 mL, 8.36 mmol) was added dropwise from an addition funnel while stirring. The mixture was allowed to warm to room temperature and stirred for 24 hours. It was then passed through a basic alumina plug using DCM as eluent to remove any unreacted methacryloyl chloride, triethylamine hydrochloride salt, and methacrylic acid. The purified product was concentrated by rotary evaporation at 23 °C to afford a colorless liquid.

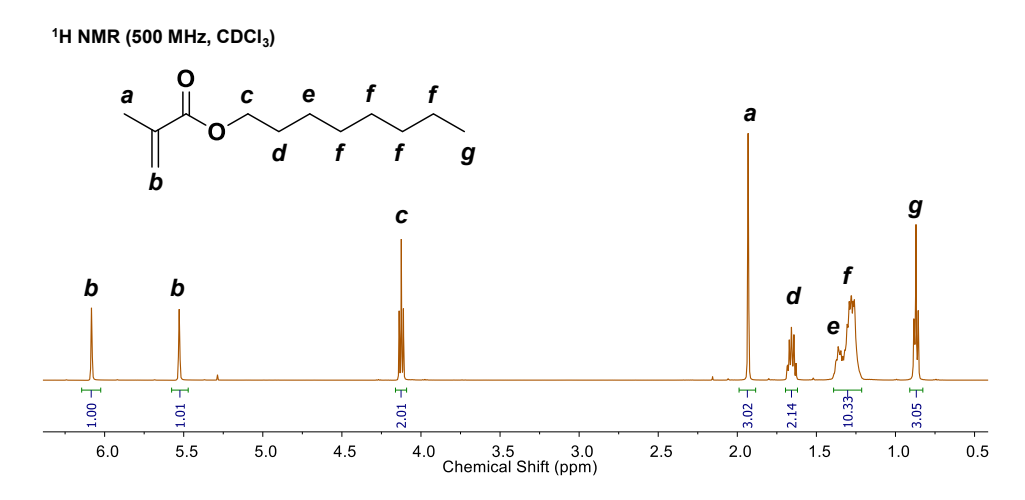


Figure S1. ¹H NMR spectrum of n-octyl methacrylate (CDCl₃, 500 MHz).

Synthesis of PTDFOMA and POMA via RAFT Polymerization. For the preparation of PTDFOMA, the chain transfer agent 4-cyano-4-(phenylcarbonothioylthio)pentanoic acid (1 eq), 2,2'-azobisisobutyronitrile initiator (0.1 eq), TDFOMA (60 eq) and TFE were mixed in a 20-mL vial equipped with a magnetic stir bar and rubber septum. The reaction mixture was degassed using dry nitrogen gas for 30 min and then stirred at 65 °C for 12 h. The polymerization was quenched by rapidly cooling the solution in liquid nitrogen and opening to air. The crude product was diluted with TFE and precipitated in methanol. The obtained polymer was re-dissolved in TFE and re-precipitated in methanol two more times to remove any unreacted monomer. A light pink solid product was obtained after drying under vacuum overnight.

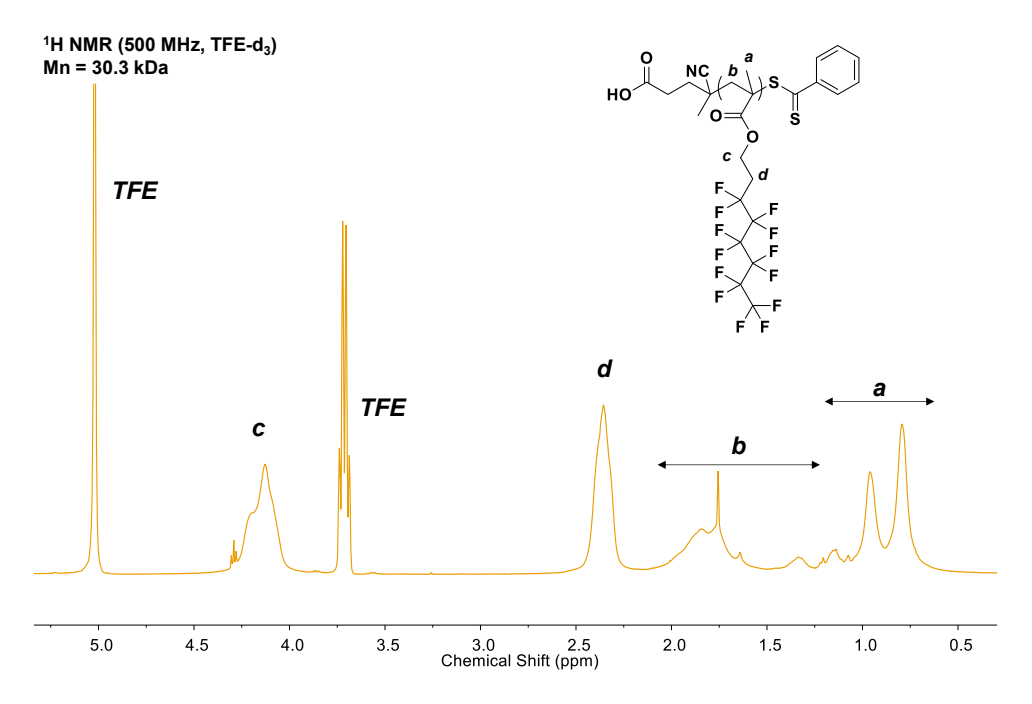


Figure S2. ¹H NMR spectrum of PTDFOMA (TFE-d₃, 500 MHz).

For the synthesis of POMA, the chain transfer agent 4-cyano-4-(phenylcarbonothioylthio)pentanoic acid (1 eq), 2,2'-azobisisobutyronitrile initiator (0.3 eq), n-octyl methacrylate (100 eq) and toluene were mixed in a 20-mL vial equipped with a magnetic stir bar and rubber septum. The reaction mixture was degassed using dry nitrogen gas for 30 min and then stirred at 70 °C for 24 h. The polymerization was quenched by rapidly cooling the solution in liquid nitrogen and opening to air. The crude product was diluted with toluene and precipitated in methanol. The obtained polymer was re-dissolved in toluene and re-precipitated in methanol two more times to remove any unreacted monomer. A light pink solid product was obtained after drying under vacuum overnight.

RAFT polymerization afforded the desired polymers as light pink solids with number-average molecular weight (M_n) values in the 30-35 kDa range estimated from ¹H NMR spectroscopy and polydispersity index of 1.04 obtained from gel permeation chromatography relative to PMMA standards.

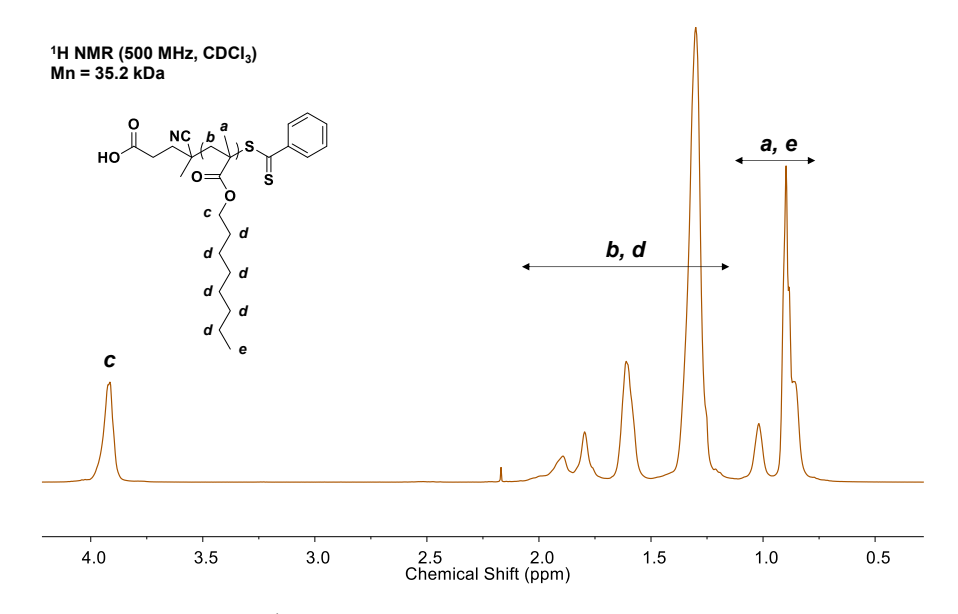


Figure S3. ¹H NMR spectrum of POMA (CDCl₃, 500 MHz).

Sample Preparation. PTDFOMA and POMA were dissolved in TFE and CHCl₃, respectively, and diluted to attain a final concentration of 1 mg/mL. The polymer solutions were individually spin-coated onto the TMDC substrates at 500 rpm for 5 s and then at 4000 rpm for 55 s. Prior to deposition, these solutions were subjected to sonication (inserting a glass vial of the polymer solution into a sonication bath) for 10 minutes at room temperature and filtered through a PTFE membrane (0.2 μ m VWR). To remove the residual solvent, the samples were vacuum-dried at room temperature for at least 18 hours. Polymer film thickness is estimated at ~ 8 nm, based on ellipsometry measurements performed on a variety of polymer films prepared from identical spin-coating conditions on Si wafers as those on MoS₂. Film uniformity is good, with the RMS roughness on the same order as the underlying MoS₂ substrate (1.82 nm, 2.09 nm, 1.35 nm for bare, PTDFOMA, and POMA, respectively.)

Photoluminescence (PL) Measurement. PL spectra were collected using an inverted microscope (Nikon TE 2000) in an epi-illumination configuration. Excitation from a 488-nm argon ion laser (National Laser H800NAL) was directed through an objective (Zeiss Plan NeoFluar 20x, 0.5 NA) via a dichroic mirror (Semrock Di02-R488), resulting in a power density of ~150 mW/cm² at the sample plane. Sample

fluorescence was collected back through the objective and filtered by the same dichroic element followed by a long pass filter (Semrock Edge Basic 488) and was analyzed by a spectrometer with a 300 groove/mm diffraction grating (Princeton Instruments SP2300, and Pixis 100). A blank Au/Ti/SiO₂/Si substrate was measured with the same settings and used to background subtract acquired spectra images. Ambient temperature during the measurements was 22 +/-2 °C, regulated at the room level and with no additional control.

Data fitting was performed in *Mathematica* by employing NonlinearModelFit with a test function consisting of two Lorentzian components for the A and B excitons, and the convolution of a Lorentzian with a decaying exponential for the trion component, with the overall form given by:

$$I(E) = \left(\frac{1}{\pi} \frac{A_1 \Gamma_1}{\left(E_{tr,1} - E\right)^2 + \Gamma_1^2} \left(1 + \frac{2\varepsilon \left(E_{tr,1} - E\right)}{\left(E_{tr,1} - E\right)^2 + \Gamma_1^2}\right)\right) + \left(\frac{1}{2\pi} \frac{A_2 \Gamma_2}{\left(E_{tr,2} - E\right)^2 + \Gamma_2^2}\right) + \left(\frac{1}{2\pi} \frac{A_3 \Gamma_3}{\left(E_{tr,3} - E\right)^2 + \Gamma_3^2}\right)$$
(S1)

where subscripts 1,2,3 indicate parameters pertaining to the trion, A, and B excitons, respectively, A_x are scaling parameters, Γ_x are width, $E_{tr,x}$ are the peak positions, E is the photon energy, and ε is a mixing parameter.

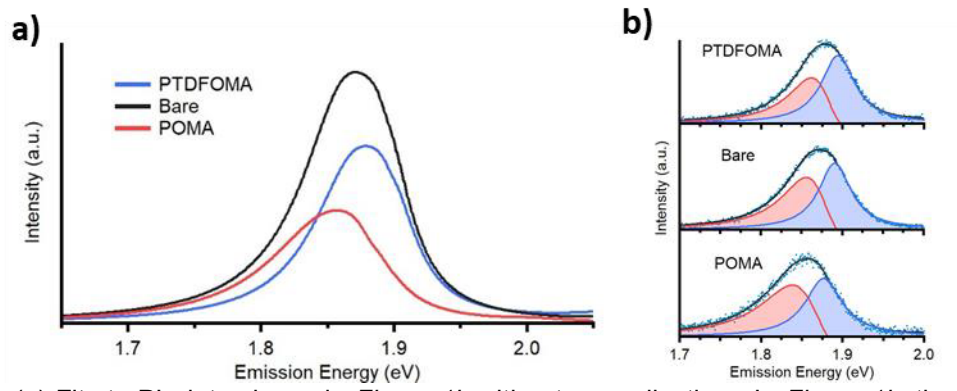


Figure S4. (a) Fits to PL data shown in *Figure 1b* without normalization. In *Figure 1b*, the intensity was normalized to unit area in the energy region examined. (b) Fit curves overlaid on raw data.

Table S1. Summary of fit parameters. All parameters are given in terms of eV, except the A parameters which are expressed in eV-counts.

	3	A_1	Γ_1	$E_{tr,1}$	A_2	Γ_2	$E_{tr,2}$	A ₃	Γ_3	$E_{tr,3}$
Bare	0.0573	3.16	0.0441	1.87	3.77	0.0494	1.89	0.0793	0.0557	2.08
POMA	0.124	1.48	0.0584	1.87	1.69	0.0551	1.88	0.0530	0.0625	2.01
FOMA	0.0629	1.76	0.0419	1.88	2.76	0.0501	1.89	0.478	0.120	2.09

Calculation of Electron Density. Trion emission is proportional to the trion population in MoS_2 , which form according to the reaction $Ex + e^- \rightarrow Tr$, where Ex is an exciton and Tr is a trion. The fact that this reaction takes electron as a reactant can be used to relate trion population to electron density, employing the mass action law for trions:²

$$\frac{N_X n_{el}}{N_{X^-}} = \left(\frac{4m_X m_e}{\pi \hbar^2 m_{X^-}}\right) k_B T E x p \left(\frac{-E_b}{k_B T}\right) \tag{S2}$$

where m_e (0.35 m_0), m_X (0.8 m_0), and m_{X^-} (1.15 m_0), are the effective masses of the electron, exciton, and negative trion, respectively, and m_0 is the free electron rest mass. N_X , N_{X^-} and n_{el} are the exciton, trion, and free electron population densities, and E_b is the trion binding energy. The PL intensities of trion and exciton can be expressed in terms of their respective populations are as follows:

$$I_X = A\gamma_{ex}N_X \tag{S3}$$

$$I_{X^-} = A \gamma_{tr} N_{X^-} \tag{S4}$$

where γ_{ex} and γ_{tr} are the radiative decay rates of excitons, and trions, respectively, and A is a constant related to experimental collection efficiency.⁴ The ratio of trion PL intensity (S4, from deconvolution) to total PL intensity (sum of trion and exciton intensities, S3 and S4), can then be combined with S2 to determine the electron density,

$$n_{el} = \frac{I_{X^{-}}}{I_{tot} - I_{X^{-}}} \frac{\gamma_{ex}}{\gamma_{tr}} \left(\frac{4m_X m_e}{\pi \hbar^2 m_{X^{-}}}\right) k_B T Exp\left(\frac{-E_b}{k_B T}\right) \tag{S5}$$

where we used the value for $\frac{\gamma_{tr}}{\gamma_{ex}}$ of 0.15.⁴

Kelvin Probe Force Microscopy (KPFM) Measurement. Samples were analyzed using a Dimension Bioscope AFM with a Nanoscope IIIa controller, using 2-pass lift mode AM-KPFM, and with vibration isolation via a Minus K BM-8 platform placed within a Herzan The Crypt acoustic enclosure. AppNano ANSCM-PT probes were used for all measurements, which consist of a ~225 mm long Si cantilever coated with PtIr, resulting in tips with ~30 nm radius and a resonant frequency of ~75 kHz. Measurements were performed with a scan size of 10 μm, at speeds between 1.0 and 1.5 Hz, and with a lift height of 30 nm. Analysis of topography images was performed in *Gwyddion*, by performing row alignment and plane subtraction, and analysis of SPC images by row alignment only or no processing. KPFM images were used to form distributions by first removing grain boundaries, visible as high work function lines in *Figure 2a*, by generating a mask to exclude those data points. The work function of the tip was established by measuring the SPC of highly oriented pyrolytic graphite (HOPG), and using a value of 4.65 eV for HOPG.⁵

References

- (1) Pagaduan, J. N.; Hight-Huf, N.; Datar, A.; Nagar, Y.; Barnes, M.; Naveh, D.; Ramasubramaniam, A.; Katsumata, R.; Emrick, T. Electronic Tuning of Monolayer Graphene with Polymeric "Zwitterists." *ACS Nano* **2021**, *15* (2), 2762–2770.
- (2) Ross, J. S.; Wu, S.; Yu, H.; Ghimire, N. J.; Jones, A. M.; Aivazian, G.; Yan, J.; Mandrus, D. G.; Xiao, D.; Yao, W.; et al. Electrical Control of Neutral and Charged Excitons in a Monolayer Semiconductor. *Nat. Commun.* **2013**, *4*, 1–6.
- (3) Cheiwchanchamnangij, T.; Lambrecht, W. R. L. Quasiparticle Band Structure Calculation of Monolayer, Bilayer, and Bulk MoS₂. *Phys. Rev. B* **2012**, *85* (20), 205302.
- (4) Mouri, S.; Miyauchi, Y.; Matsuda, K. Tunable Photoluminescence of Monolayer MoS2 via Chemical Doping. *Nano Lett.* **2013**, *13* (12), 5944–5948.
- (5) Sommerhalter, C.; Matthes, T. W.; Glatzel, T.; Jäger-Waldau, A.; Lux-Steiner, M. C. High-Sensitivity Quantitative Kelvin Probe Microscopy by Noncontact Ultra-High-Vacuum Atomic Force Microscopy. *Appl. Phys. Lett.* **1999**, *75* (2), 286–288.